# An Adaptive Anti-Brownian Electrokinetic Trap with Real-Time Information on Single-Molecule Diffusivity and Mobility

**Quan Wang and W. E. Moerner***

Department of Chemistry, Stanford University, Mail Code 5080, Stanford, California 94305-5080, United States

**ABSTRACT** We present the design and implementation of an adaptive Anti-Brownian ELectrokinetic (ABEL) trap capable of extracting estimates of the diffusion coefficient and mobility of single trapped fluorescent nanoscale objects such as biomolecules in solution. The system features rapid acousto-optic scanning of a confocal excitation spot on a 2D square lattice to encode position information on the arrival time of each detected photon, and Kalman filter-based signal processing unit for refined position estimation. We demonstrate stable trapping of multisubunit proteins ($D \approx 22\ \mu m^2/s$) with a count rate of 6 kHz for as long as 15 s and small single-stranded DNA molecules ($D \approx 118\ \mu m^2/s$) at a 15 kHz count rate for seconds. Moreover, we demonstrate real-time measurement of diffusion coefficient and electrokinetic mobility of trapped objects, using adaptive tuning of the Kalman filter parameters.

**KEYWORDS:** ABEL trap · Kalman filter · single molecule · fluorescence microscopy · diffusion coefficient · electrokinetic mobility

Single-molecule spectroscopy in solution offers the unique opportunity to study biomolecules in a close-to-native environment, free of ensemble averaging and the possible perturbative effects of surface attachment or encapsulation.[1] However, Brownian motion poses a serious limitation on the observation times of nanoscale objects in the aqueous phase. Characteristic dwell times of typical protein molecules in a diffraction-limited confocal volume (as in fluorescence correlation spectroscopy, FCS) are on the order of several milliseconds, precluding the study of long time dynamics. Moreover, simple diffusion through a focused spot causes each molecule to experience different paths through the Gaussian-shaped focus and thus to have a fluorescence signal with ill-defined brightness.

Faced with such limitations, there has been tremendous interest in methodology development to trap and/or track single nano-objects in solution in recent years, for example, by using various methods to follow the Brownian object,[2−7] by enhancement of the field gradient in a dielectric optical trap,[8] by engineering the electrostatic potential around charged nanoscale objects,[9,10] and by electrokinetic trapping with real-time feedback in the anti-Brownian electrokinetic (ABEL) trap,[11,12] the method treated here.

The ABEL trap works by real-time monitoring of the position of the diffusing molecule and applying a set of voltages so that the induced electrokinetic drift approximately cancels the Brownian displacement within the bandwidth of the feedback system. Since initial first implementations which used a fast CCD camera as position detector and software-based signal processing,[13] the technology has shifted to revolving beam-based position sensing and an all-hardware, analog feedback system,[14] with much improved detection efficiency, feedback bandwidth, and spatially uniform optical intensity in the trapping region on time scales longer than the revolution time. Such a system has enabled real-time monitoring of photodynamical processes of single photosynthetic antenna proteins[15] as well as measurements of ATP binding stoichiometry in multisubunit enzymes.[16] Most recently, we have theoretically outlined an optimal trapping strategy that utilizes a grid-scanning pattern of the excitation beam to encode more specific position information on every detected photon, and a Kalman filter-based signal-processing algorithm for optimal online estimation of position;[17] we showed by Monte Carlo simulations that tighter trapping can be expected as compared to previous schemes.

In this paper we report an advanced, adaptive ABEL trap based on such an optimal strategy. (A related system, which pushes

* Address correspondence to wmoerner@stanford.edu.

Received for review April 22, 2011 and accepted May 25, 2011.

**Published online May 25, 2011**
10.1021/nn2014968

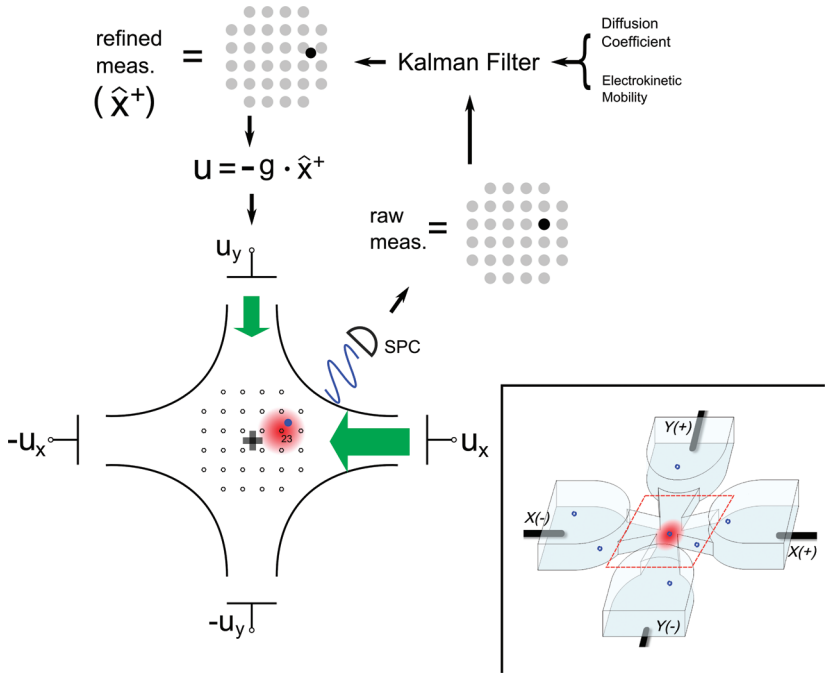


**Figure 1. Working principle of the ABEL trap. Right bottom inset: 3D view of the microfluidic device[34] used to implement the ABEL trap. The depth of the channel near the center (inside red dashed square) is ~600 nm, designed to confine the object along the z-dimension as well as to support a strong electrokinetic flow for actuation. Macroscopic electrodes inserted into the fluid channels are also shown. *x*–*y* Brownian motion is suppressed by feedback control (red dashed area, main figure): A focused laser spot (red Gaussian) rapidly scans through a 32-point grid on a square lattice through a knight's tour pattern (see Figure 2a for the pattern and the order of beam positions). When the excitation beam is close to the real position of a diffusing object (blue dot), a fluorescence photon can sometimes be detected by a single photon counter (SPC). The position of the beam at the photon detection event (in the example, position number 23) is taken to be the raw measurement (y) of the object's position. The raw measurement is then refined by a Kalman filter, given the diffusivity and mobility information of the object, to produce a better estimate ($\hat{x}^+$). A pair of voltages are calculated and applied to four electrodes in the solution to induce a restoring electrokinetic flow (green arrows show the flow decomposed into its Cartesian components) to bring the object back to the center (black cross). This process repeats for every detected photon.**

the limit of electrokinetic trapping in solution to single fluorophores has been recently described.[18,19]) We present a new feedback algorithm based on an *adaptive* Kalman filter to extract estimates of the diffusion coefficient and electrokinetic mobility of trapped objects in real time. As experimental demonstrations, we first show the stable trapping of single labeled proteins and small oligonucleotides with low count rate and subsequently demonstrate the adaptive feature of the trap on fluorescently labeled nanospheres.

Figure 1 illustrates the working principle of a photon-by-photon, Kalman filter-based ABEL trap, which is generally implemented in a microfluidic sample cell which is thin in the *z*-direction (see inset and caption); therefore, the trap suppresses *x*–*y* Brownian motion. To trap single molecules that are generally dim and fast-diffusing, it is critical to most efficiently extract position information in real time. In our design, the excitation beam traverses a 32-point grid through a knight's tour pattern (Figure 2a).[17,20] Each detected fluorescent photon, depending on its arrival time, is mapped to the current position of the excitation beam on the grid. This position (which we call the raw measurement *y*) serves as a reasonably good estimate of the actual position of the molecule, since the probability of emitting a photon is largest when the molecule overlaps with the center of the excitation beam. We use a Kalman filter and a Langevin equation of motion for the diffusing molecule in the applied field to refine the raw measurement. The Kalman filter,[21] well-known in control system theory, efficiently and optimally estimates the internal states of a linear dynamic system from a series of noisy measurements,[22] provided that an accurate model of the system dynamics is available, and is perfectly applicable to the real-time position estimation problem in the ABEL trap. A detailed analysis can be found in ref 17. The algorithm in its entirety is included in the Supporting Information.

For every detected photon, the Kalman filter outputs a refined estimate of position (posterior estimate, termed $\hat{\mathbf{x}}^+$), which is optimal in the best-case scenario. Because the particle position is then approximately known, voltages are computed (with gain *g*) which generate an applied field vector (**u**) to induce an electrokinetic flow in the opposite direction from the trap center, producing the required negative feedback for approximate cancellation of Brownian motion.

The Kalman filter assumes perfect knowledge of the system model parameters (in the case of the ABEL trap,

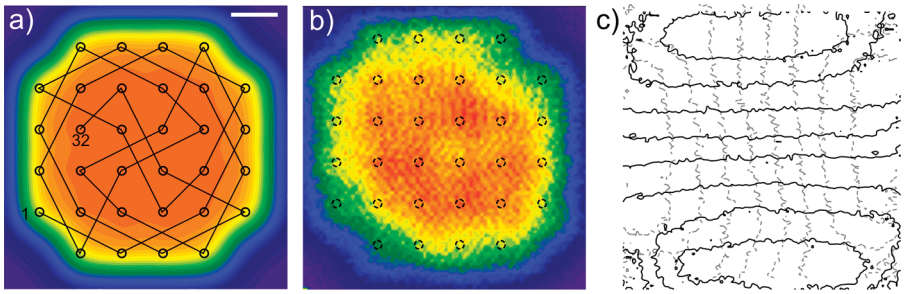


**Figure 2. The beam traversal pattern. (a) The designed beam trajectory and calculated time-averaged intensity over the trapping region (scale bar = 0.5 $\mu$m). (b) Actual time-averaged intensity map, acquired by scanning a 100 nm fluorescent bead over the trapping region. (c) Position sensitivity of the apparatus, shown as contour plots of measured position (interval: 0.25 $\mu$m) of the fluorescent bead in panel b. Position response is linear and orthogonal in an area of 2 $\mu$m $\times$ 2 $\mu$m near the center.**

the diffusion coefficient $D$ and electrokinetic mobility $\mu$ of the object in the trap). Errors in modeling lead to performance degradation, as was analyzed in early development of the Kalman filter.[23] To address this problem, various adaptation methods have been proposed[24,25] which aim to estimate the model parameters together with estimation of states. Algorithms of this kind include maximum likelihood estimators,[26] multimodel Kalman filtering,[27] and innovation-based methods.[28] Although not as mathematically rigorous as the maximum likelihood approach, the innovation-based methods (to be described below) are less computationally intensive and are well suited for practical real-time applications.

## RESULTS AND DISCUSSION

**Adaptive Trapping Algorithm Based on Innovation "Whitening".** We formulate our adaptive trapping algorithm on the basis of the innovation approach. For clarity, we restrict the following discussion to one Cartesian component on the 2D plane. The "innovation" (or measurement residue) sequence (defined as the difference between raw measurement and prior estimate, $r_k = y_k - \hat{x}_k^-$) represents the new information available in measurement $y_k$, that is, the new information arising from photon detection at time $k$ when the beam is at position $y$. The optimality of the Kalman filter is reflected in the fact that if the model is accurate, the innovation at time $k$ is statistically independent of all the past or future innovations, that is, $r_i$ ($i$ = 1, 2, 3, ...) is an uncorrelated white noise sequence. Mathematically, we have, with $E$ the expectation,

$$E(r_k \cdot r_{k+j}) = 0, \quad \text{for } j > 0 \qquad (1)$$

Any error in modeling would result in correlated (nonwhite) innovation sequences. It can be shown (see Supporting Information for derivation) that in the case of the ABEL trap, an inaccurately modeled $D$ (parametrized by the fractional error $\alpha = \Delta D/D$) would cause correlations in the innovation sequence approximated by

$$E(r_k \cdot r_{k+j}) \approx -\frac{\alpha \cdot (2D\overline{\Delta t})}{\bar{K} \cdot (2 - \bar{K})} \cdot (1 - \bar{K})^j \qquad (2)$$

where $\overline{\Delta t}$ is the average duration of the feedback kicks, and $\bar{K}$ is the averaged Kalman gain during trapping. Similarly, a modeling error in the mobility $\mu$ (parametrized by the fractional error $\beta = \Delta\mu/\mu$) would produce correlated innovation sequence approximated by

$$E(r_k \cdot r_{k+j}) \approx \beta \cdot (g\mu\overline{\Delta t}) \cdot (2D\overline{\Delta t}) \cdot (1 - \mu g\overline{\Delta t})^{j-1} \qquad (3)$$

where $g$ is the feedback gain. It can be seen from eqs 2 and 3 that nonzero autocorrelation in the innovation sequence contains information about the underlying true model parameters. Moreover, owing to the different time dependence of displacements due to electrokinetic flows ($\propto \Delta t$, the time between photon detection events) and due to Brownian motion ($\propto (\Delta t)^{1/2}$), the effect of modeling error in $D$ and $\mu$ can be separated, when the autocorrelation is examined at different time lags (see Supporting Information for details). Specifically, short time correlations are mainly caused by errors in the modeled diffusion coefficient, while long time correlations are mostly related to errors in modeling the mobility.

Figure 3 shows Monte Carlo simulation results of the short lag time (defined in the simulation as $\tau < 100$ $\mu$s, termed *stCorr*, Figure 3a) and the long lag time (300 $< \tau < 2000$ $\mu$s, termed *ltCorr*, Figure 3b) correlations of the innovation sequence as a function of fractional modeling error. It can be seen that the contours are almost orthogonal near the origin in the parameter space, reflecting good separation of the effect caused by the two parameters. The adaptive algorithm works by real-time tuning of $D$ and $\mu$ in the direction that respectively minimizes *stCorr* and *ltCorr*, as detailed in the Supporting Information, a process which we term "correlation whitening". Figure 3c shows the comparison between the autocorrelation of the innovation sequence for the correct model (gray upper) and for a situation where $D$ is underestimated and $\mu$ is overestimated (red lower). Figure 3d illustrates the adaptation process on the parameter space from an actual experimental implementation described below in Figure 6a.

In studying single molecules in aqueous buffers, both the diffusion coefficient $D$ and electrokinetic

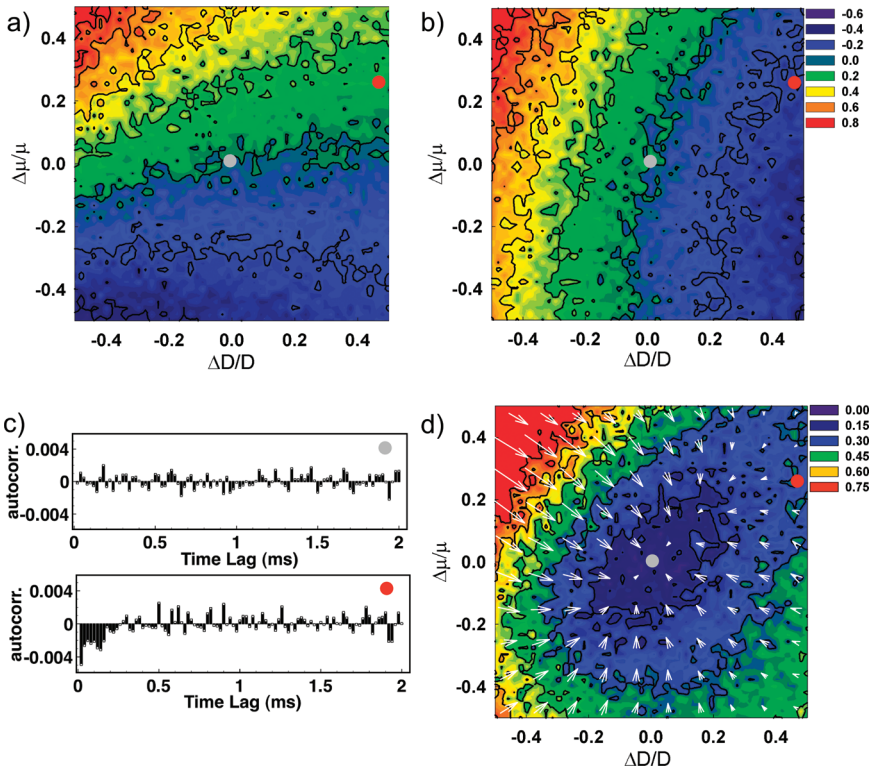


**Figure 3. Adaptive trapping by whitening the autocorrelation of the innovation sequence. (a) Long time correlation of the innovation sequence as a function of model deviation showing the primary dependence on mobility error. (b) Short time correlation of the innovation sequence as a function of model deviation showing the primary dependence on the diffusion error. (c) Example autocorrelations of the innovation sequences. Gray circle: accurate model. Red circle: *D* overestimated by 45%, $\mu$ overestimated by 25%. (d) Simulated adaptation trajectory on the parameter space by correlation whitening using parameters similar to the experiment in Figure 6, where the gray and red dots correspond to the two cases in panel c.**

mobility $\mu$ may be heterogeneous and time-dependent in general. Previous efforts to estimate $D$ and $\mu$ were achieved by offline postprocessing.[12,17] Our new adaptive trapping method offers two major advantages over offline methods: first, because of its real-time nature, the information learned about each object in the trap is immediately used to improve subsequent trapping of the object; second, it becomes possible to monitor a change in either of the two dynamical properties in real time (*i.e.,* a change in diffusion coefficient of a macromolecule due to binding/unbinding events, or a change in mobility due to changes in charge state). We note that the starting estimates ($D_0$, $\mu_0$) for the Kalman filter can be chosen by performing a bulk measurement using fluctuation correlation spectroscopy[29,30] or other methods.

**The Knight's Tour Beam Scanning Pattern.** Figure 2b illustrates the average intensity profile of an actual knight's tour scan, acquired by $x-y$ scanning a fluorescent bead at the focal plane using a piezoelectric stage. A reasonably good agreement with the designed pattern (Figure 2a) is achieved. Figure 2c shows the position sensitivity of the trap, acquired by averaging the raw measurements (15 ms averaging time) as the bead is scanned over the trapping area. The measured position is linear in both the $x$ and $y$ dimensions over an area of 2 $\mu$m $\times$ 2 $\mu$m near the center of the trapping region, suggesting the possibility of using the apparatus as a tracking device[31] with time resolution limited only by photon counting rate.

**Trapping Fluorescently Labeled Proteins and Oligonucleotides.** To compare the knight's tour/Kalman approach with previous work, we first implement the trap without adaptation, using model parameters from a FCS measurement. We trapped single molecules of the chaperonin protein from *Methanococcus maripaludus* (Mm-cpn), a large multisubunit enzyme with a molecular weight of about 1 MDa (~15 nm in diameter).[32] These molecules are stably trapped when labeled with just a single Atto647N fluorophore, with a detected count rate of 6 kHz (average pumping intensity 750 W/cm$^2$) and a signal-to-background ratio of 1:1 (Figure 4). Occasionally, an enzyme labeled with two fluorophores is observed as two brightness levels (third trace from the top in Figure 4a). In this measurement, the majority of the background signal arises from autofluorescence of the glass coverslip that seals the microfluidic trapping cell. The long trapping times achieved in this experiment reflect the superior performance of the trap, but are also largely due to the photostability of Atto647N. This demonstrated capability of the ABEL trap offers unprecedented long observation times for studying single enzymes in solution without surface immobilization. Moreover,

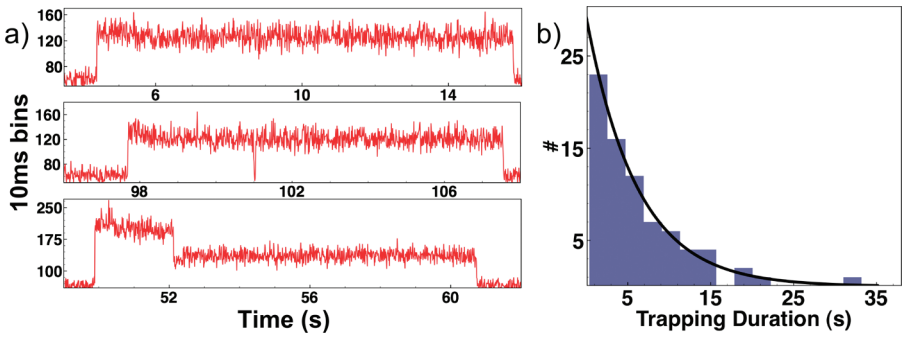


**Figure 4. Trapping single multisubunit enzyme molecules (Mm-cpn, labeled with Atto647N) with optimal filtering: (a) example trajectories of detected fluorescence counts in 10 ms bins; (b) histogram of trapping durations.**

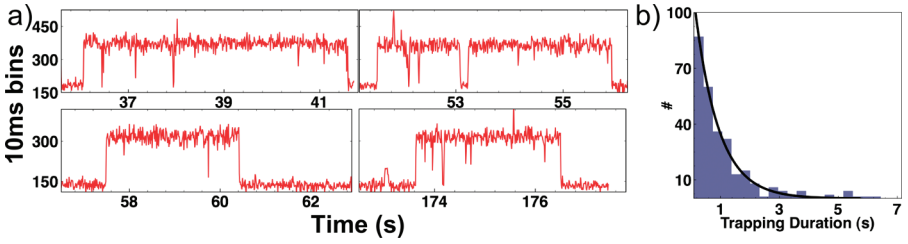


**Figure 5. Trapping single 30 base oligonucleotides, labeled with a single Atto647N fluorophore. (a) Example trajectories of detected fluorescence counts in 10 ms bins. (b) Histogram of trapping durations.**

the molecule is trapped in a region of relatively uniform intensity, as evidenced by the constant emission signals.

We next trapped single Atto647N-labeled oligonucleotides composed of 30 thymine bases (30T, AnaSpec, Inc.). These single-stranded DNA biopolymers have a molecular weight of 9 kDa and linear dimensions of 9 nm along the chain. A bulk measurement of the diffusion coefficient with fluorescence correlation spectroscopy yielded a value of 118 ± 25 $\mu m^2/s$ (Supporting Information, Figure S4). Using a higher pumping intensity (1.7 $kW/cm^2$), the 30T oligos can be stably trapped with a count rate of 15 kHz and the same signal-to-background ratio as Mm-cpn (Figure 5). In this case, however, the average trapping time, extracted by exponential fitting of the burst duration histogram, is 0.97 s.

**Real-Time Measurement of Diffusion Coefficient and Mobility for Fluorescent Beads.** To demonstrate the ability of the adaptive trap to provide real-time measurement of diffusion coefficient and electrokinetic mobility, we used fluorescently doped polystyrene beads (Invitrogen) as a proof-of-principle, because of their known sizes and superior signal to background. Figure 6a shows data from one 100 nm diameter bead in the trap. In this experiment, the Kalman filter initially operates with user supplied model parameters ($D$ = 11.2 $\mu m^2/s$, $\mu_x$ = $\mu_y$ = 500 $\mu m/s/V$), until at 4.7 s, the adaptation algorithm is enabled. As can be seen from the corresponding plot of real time diffusion coefficient and the two mobility components (red and black), all three adapted model parameters responded, in this case, to a lower value ($D \approx 3.8\ \mu m^2/s$, $\mu_x \approx 350\ \mu m/s/V$, $\mu_y \approx 250\ \mu m/s/V$). The autocorrelation of the innovation sequence, calculated from before (red region) and after (green region) the adaptation, are plotted in Figure 6b. A much "whitened" autocorrelation is observed as the result of the adaptive tuning. Good qualitative agreement between experiment and simulation (Figure 3c, generated from parameters used in Figure 6a) can be seen. It is interesting to note that in the case of this particular bead, $\mu_x$ and $\mu_y$ adapt to different values, possibly reflecting the inhomogeneity of the flow along the two dimensions in the microfluidic environment. A distribution of measured diffusion coefficients from this 100 nm bead mixture, collected from 30 beads, is plotted in Figure 6d (blue curve), with a mean value of 3.8 $\mu m^2/s$, in reasonably good agreement with a value calculated from the Stokes–Einstein equation, which is 4.4 $\mu m^2/s$.

Similar measurements were performed on 26 nm diameter beads in solution, and Figure 6c shows a snapshot, where several beads with different diffusion coefficients and brightness are captured by the trap. We found that bright objects generally correlate with lower diffusion coefficients, presumably because larger beads contain more dye molecules. To rule out the possibility that the measured diffusion coefficient is affected by the object's brightness, we trapped a single bead and modulated its brightness by changing the excitation power, and minimal influence of brightness on the measured diffusion coefficient is seen (Supporting Information, Figure S5). In contrast to the 100 nm bead case, the 26 nm beads appear to be less

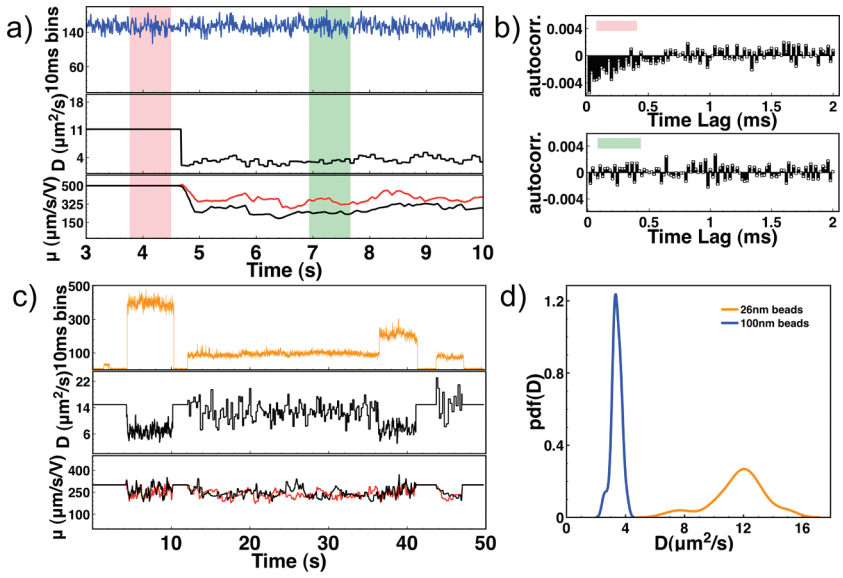


**Figure 6. Adaptive trapping of fluorescent polystyrene beads of different sizes. (a) Trapping signals from one 100 nm bead. The simultaneously recorded intensity trace (upper) and extracted diffusion coefficient (middle) and electrokinetic mobility (lower) are shown. At around 4.7 s, adaptation is enabled, before which user supplied initial parameters were used (see text for details). (b) Autocorrelation of measured innovation sequences, from corresponding regions shown in panel a. (c) Fluorescence emission from several trapped beads with nominal size of 26 nm, with real-time extracted diffusion coefficient and electrokinetic mobility as in panel a. Each bead is actively released to allow another bead to occupy the trap (except at around 37 s, where a brighter bead diffused in and replaced the previous occupant). Update rates in $D$ and $\mu$ correlate with intensity since adaptive tuning is performed for every fixed number of detected photons. Values of $D$ and $\mu$ are independent of count rate (Supporting Information, Figure S5). (d) Histograms of the measured diffusion coefficients for the 100 nm (blue) and 26 nm beads (orange).**

homogeneous in size, indicated by the broader distribution of measured diffusion coefficients (Figure 6d, orange curve). This inhomogeneity agrees qualitatively with the manufacturer's specification (20% size polydispersity for the 26 nm beads *versus* 5% for 100 nm beads). The measured electrokinetic mobility of the beads varies slightly between trapping cells, but the average value of 250 $\mu$m/s/V, acquired from the adaptive trapping of the 26 nm beads, agrees favorably with a bulk measurement by FCS, under identical surface preparation conditions (Supporting Information, Figure S6).

The precision of the diffusion coefficient/mobility obtained by our adaptive Kalman filtering method depends on several factors: first of all, the precision of measuring the scan grid spacing ($a$) and the laser beamwaist ($w$). The grid spacing defines the length scale so that if not characterized accurately, systematic errors in estimating both $D$ and $\mu$ will occur. The beamwaist defines the error variance of individual measurements and is critical in the calculation of the Kalman gain ($K_k$). An inaccurate beamwaist would thus affect the estimation precision of the diffusion coefficient (eq 2), but not the mobility. Second, and perhaps more importantly, the presence of background photons would greatly affect the estimation of the diffusion coefficient. Intuitively, the fact that every detected photon has a certain probability to originate from background would increase the measurement noise accordingly (the measurement error variance would be greater than $(w/2)^2$). The effect is qualitatively similar to the case of an underestimated beamwaist, as discussed above. A significant amount of background photons would also introduce non-Gaussian statistics to the problem, in which case the Kalman filter ceases to be a truly optimal solution and complete treatment is generally beyond efficient implementation. To retain the favorable computational complexity of the Kalman filter while taking background photons into account, we used a built-in "innovation filter" to reject photons with large measurement residues (over a user defined threshold),[33] since these are most likely to be generated by background photons (see Supporting Information for details). While the extracted $D$ and $\mu$ can be particularly helpful in sensing changes in these parameters in real time, the absolute accuracy of both depend on the effects mentioned above, and measurements on a calibration object may be necessary for precise values.

## CONCLUSION

We have presented a detailed design and implementation of an advanced ABEL trap for single nanoscale objects in solution. With the efficient and optimal signal processing strategy provided by Kalman filtering, we have achieved stable trapping of single large multisubunit enzymes (molecular weight: 930 kDa) as well as single small oligonucleotides (molecular weight: 9 kDa) labeled with a single fluorescent dye molecule, with a signal-to-background ratio of only 1:1.

We expect further improvement of the trap's capability to localize smaller objects when using an all-quartz cell design with lower background.

We also outlined a strategy to estimate the diffusion coefficient and electrokinetic mobility of trapped object in real-time, using adaptive tuning to whiten the innovation sequence. We demonstrated the technique on fluorescently labeled polystyrene beads of different sizes. The adaptive capability of the trap ensures that the estimation algorithm stays optimal for different objects which may enter the trap. This approach could also facilitate the detection of single molecule binding-unbinding events in the ABEL trap when such events change the diffusion coefficient of the trapped object.

## METHODS

**Beam Scanning Pattern.** We use a pair of acousto-optical beam deflectors (AOBD, AA Optoelectronics, Fr, MT110-B54A1.5-VIS) to create the scanning pattern in the focal plane. With $w$ = 0.4 $\mu$m and $a$ = 0.5 $\mu$m, we achieve a Rayleigh range (focal depth) of 0.8 $\mu$m that matches well with the depth of the microfluidic cell in the $z$ direction and an overall $x-y$ trapping region of 2.5 $\mu$m $\times$ 2.5 $\mu$m in size. The actual frame rate is 39 kHz (point dwell time of 800 ns). Full optical details are presented in the Supporting Information.

**Algorithm Implementation.** The photon-by-photon Kalman filter algorithm and the innovation-based adaptation scheme are implemented directly on a Field Programmable Gate Array (FPGA, NI PCI-7842R) using the LabView FPGA module (version 2009). User control and data collecting software are written in LabView as well. The program runs on a PC computer hosting the FPGA board and communicates with the FPGA board *via* DMA (direct memory access) channels. All trapping parameters are easily adjustable in real time. The delay time between photon detection and the output feedback voltage is at most 2 $\mu$s. Full details about FPGA programming can be found in the Supporting Information.

**Sample Preparation.** Mm-cpn molecules are conjugated with Atto647N-NHS (ATTO-TEC GmbH) through surface exposed lysine residues and purified with P30 size exclusion columns (BioRad). Before trapping, the sample is diluted to ~50 pM concentration in buffer solution containing 20 mM HEPES (pH 7.5), 50 mM NaCl, 5 mM $MgCl_2$, 5% (v/v) glycerol. Prior to injection into the microfluid cell, the diluted sample is further mixed with 10% (v/v) POP-6 (without denaturant, Applied Biosystems), a solution for dynamic coating of the microfluidic cell. Otherwise, sticking of Mm-cpn molecules to walls of the microfluidic environment is observed. 30T-Atto647N oligonucleotides are purchased from AnaSpec (Fremont, CA) and diluted to ~100 pM in buffer solution containing 40 mM Tris acetate, 1 mM EDTA, and 12.5 mM $MgCl_2$. Additives to reduce photo bleaching were not required. Fluorescent beads are purchased from Invitrogen, sonicated for 10 min, diluted to ~100 pM in Nanopure water and injected into the trapping cell.

*Acknowledgment.* We thank G. Wallraff and S. Swanson for providing the Atto647N labeled 30T sample, Y. Jiang for discussions and help with Figure 1, L. Lau for suggestions on the experimental setup, and R. Goldsmith and N. Douglas for the Mm-cpn-Atto647N sample. This work was supported in part by the Division of Chemical Sciences, Geosciences, and Biosciences, Office of Basic Energy Sciences of the U.S. Department of Energy through Grant DE-FG02-07ER15892.

*Supporting Information Available:* Details of the trapping algorithms, optical setup, FPGA programming, Monte Carlo simulation, and control experiments. This material is available free of charge *via* the Internet at http://pubs.acs.org.

## REFERENCES AND NOTES

1. Zander, C.; Enderlein, J.; Keller, R. A. *Single-Molecule Detection in Solution: Methods and Applications*; Wiley-VCH: Berlin, 2002.
2. Cang, H.; Wong, C. M.; Xu, C. S.; Rizvi, A. H.; Yang, H. Confocal Three Dimensional Tracking of a Single Nanoparticle with Concurrent Spectroscopic Readouts. *Appl. Phys. Lett.* **2006**, *88*, 223901.
3. Lessard, G. A.; Goodwin, P. M.; Werner, J. H. Three-Dimensional Tracking of Individual Quantum Dots. *Appl. Phys. Lett.* **2007**, *91*, 224106–3.
4. Berglund, A. J.; McHale, K.; Mabuchi, H. Feedback Localization of Freely Diffusing Fluorescent Particles Near the Optical Shot Noise Limit. *Opt. Lett.* **2007**, *32*, 145–147.
5. Juette, M. F.; Bewersdorf, J. Three-Dimensional Tracking of Single Fluorescent Particles with Submillisecond Temporal Resolution. *Nano Lett.* **2010**, *10*, 4657–4663.
6. McMahon, M. D.; Berglund, A. J.; Carmichael, P.; McClelland, J. J.; Liddle, J. A. 3D Particle Trajectories Observed by Orthogonal Tracking Microscopy. *ACS Nano* **2009**, *3*, 609–614.
7. Thompson, M. A.; Lew, M. D.; Badieirostami, M.; Moerner, W. E. Localizing and Tracking Single Nanoscale Emitters in Three Dimensions with High Spatiotemporal Resolution Using a Double-Helix Point Spread Function. *Nano Lett.* **2010**, *10*, 211–218.
8. Yang, A. H. J.; Moore, S. D.; Schmidt, B. S.; Klug, M.; Lipson, M.; Erickson, D. Optical Manipulation of Nanoparticles and Biomolecules in Sub-Wavelength Slot Waveguides. *Nature* **2009**, *457*, 71–75.
9. Krishnan, M.; Mojarad, N.; Kukura, P.; Sandoghdar, V. Geometry-induced Electrostatic Trapping of Nanometric Objects in a Fluid. *Nature* **2010**, *467*, 692–695.
10. Carlson, C. A.; Sweeney, N. L.; Nasse, M. J.; Woehl, J. C. The Corral Trap: Fabrication and Software Development. *Proc. SPIE* **2010**, *7571*, 757108.
11. Cohen, A. E.; Moerner, W. E. Method for Trapping and Manipulating Nanoscale Objects in Solution. *Appl. Phys. Lett.* **2005**, *86*, 093109.
12. Cohen, A. E.; Moerner, W. E. Suppressing Brownian Motion of Individual Biomolecules in Solution. *Proc. Natl. Acad. Sci. U.S.A.* **2006**, *103*, 4362–4365.
13. Cohen, A. E. Control of Nanoparticles with Arbitrary Two-Dimensional Force Fields. *Phys. Rev. Lett.* **2005**, *94*, 118102.
14. Cohen, A. E.; Moerner, W. E. Controlling Brownian Motion of Single Protein Molecules and Single Fluorophores in Aqueous Buffer. *Opt. Express* **2008**, *16*, 6941–6956.
15. Goldsmith, R. H.; Moerner, W. E. Watching Conformational- and Photodynamics of Single Fluorescent Proteins in Solution. *Nat. Chem.* **2010**, *2*, 179–186.
16. Jiang, Y.; Wang, Q.; Cohen, A. E.; Douglas, N.; Frydman, J.; Moerner, W. E. Hardware-Based Anti-Brownian Electrokinetic Trap (ABEL trap) for Single Molecules: Control Loop Simulations and Application to ATP Binding Stoichiometry in Multi-Subunit Enzymes. *Proc. SPIE.* **2008**, *7038*, 703807.
17. Wang, Q.; Moerner, W. E. Optimal Strategy for Trapping Single Fluorescent Molecules in Solution Using the ABEL Trap. *Appl. Phys. B: Lasers Opt.* **2010**, *99*, 23–30.
18. Fields, A. P.; Cohen, A. E. Anti-Brownian Traps for Studies on Single Molecules. *Methods Enzymol.* **2010**, *475*, 149–174.
19. Fields, A. P.; Cohen, A. E. Electrokinetic Trapping at the One Nanometer Limit. *Proc. Natl. Acad. Sci. U.S.A., Early Ed.*, published online May, 11, 2011, doi: 10.1073/pnas.1103554108.
20. Enderlein, J. Tracking of Fluorescent Molecules Diffusing Within Membranes. *Appl. Phys. B: Lasers Opt.* **2000**, *71*, 773–777.

21. Simon, D. *Optimal State Estimation: Kalman, H Infinity and Nonlinear Approaches*; John Wiley & Sons: New York, 2006.
22. Kalman, R. E. A New Approach to Linear Filtering and Prediction Problems. *J. Basic Eng.* **1960**, *82*, 35–45.
23. Heffes, H. The Effect of Erroneous Models on the Kalman Filter Response. *IEEE Trans. Autom. Control* **1966**, *11*, 541–543.
24. Mehra, R. K. Approaches to Adaptive Filtering. *IEEE Trans. Autom. Control* **1972**, *17*, 693–698.
25. Mohamed, A. H.; Schwarz, K. P. Adaptive Kalman Filtering for INS/GPS. *J. Geodesy* **1999**, *73*, 193–203.
26. Maybeck, P. S. *Stochastic Models, Estimation, and Control (Vols. I and II)*; Academic Press: New York, 1979.
27. Hanlon, P. D.; Maybeck, P. S. Multiple-Model Adaptive Estimation Using a Residual Correlation Kalman Filter Bank. *IEEE Trans. Aerosp. Electron. Syst.* **2000**, *36*, 393–406.
28. Mehra, R. K. On the Identification of Variances and Adaptive Kalman Filtering. *IEEE Trans. Autom. Control* **1970**, *15*, 175–184.
29. Arbour, T. J.; Enderlein, J. Application of Dual-Focus Fluorescence Correlation Spectroscopy to Microfluidic Flow-Velocity Measurement. *Lab Chip* **2010**, *10*, 1286–1292.
30. Muller, C. B.; Loman, A.; Pacheco, V.; Koberling, F.; Willbold, D.; Richtering, W.; Enderlein, J. Precise Measurement of Diffusion by Multicolor Dual-Focus Fluorescence Correlation Spectroscopy. *Eur. Phys. Lett.* **2008**, *83*, 46001.
31. Sahl, S. J.; Leutenegger, M.; Hilbert, M.; Hell, S. W.; Eggeling, C. Fast Molecular Tracking Maps Nanoscale Dynamics of Plasma Membrane Lipids. *Proc. Natl. Acad. Sci. U.S.A.* **2010**, *107*, 6829–6834.
32. Zhang, J.; Baker, M. L.; Schroder, G. F.; Douglas, N. R.; Reissmann, S.; Jakana, J.; Dougherty, M.; Fu, C. J.; Levitt, M.; Ludtke, S. J.; *et al*. Mechanism of Folding Chamber Closure in a Group II Chaperonin. *Nature* **2010**, *463*, 380–384.
33. Grewal, M. S.; Andrews, A. P. *Kalman Filtering: Theory and Practice Using MATLAB*; John Wiley & Sons: New York, 2002.
34. Cohen, A. E.; Moerner, W. E. The Anti-Brownian Electrophoretic Trap (ABEL trap): Fabrication and Software. *Proc. SPIE* **2005**, *5699*, 296–305.